CORA Cork Open Research Archive
Cartlann Taighde Oscailte Chorcaí

Title	Hardware reduction in digital delta-sigma modulators via error masking - part I: MASH DDSM
Authors	Ye, Zhipeng;Kennedy, Michael Peter
Publication date	2009-04
Original Citation	Ye, ZP, Kennedy, MP (2009) 'Hardware Reduction In Digital Delta-Sigma Modulators Via Error Masking-Part I: Mash Ddsm'. Ieee Transactions On Circuits and Systems I-Regular Papers, 56 (4):714-726.
Type of publication	Article (peer-reviewed)
Link to publisher's version	10.1109/TCSI.2008.2003383
Rights	©2009 IEEE. Personal use of this material is permitted. However, permission to reprint/republish this material for advertising or promotional purposes or for creating new collective works for resale or redistribution to servers or lists, or to reuse any copyrighted component of this work in other works must be obtained from the IEEE.
Download date	2024-04-20 06:21:49
Item downloaded from	https://hdl.handle.net/10468/132

UCC
University College Cork, Ireland
Coláiste na hOllscoile Corcaigh

Hardware Reduction in Digital Delta–Sigma Modulators Via Error Masking—Part I: MASH DDSM

Zhipeng Ye, *Student Member, IEEE*, and Michael Peter Kennedy, *Fellow, IEEE*

***Abstract*—Two classes of techniques have been developed to whiten the quantization noise in digital delta–sigma modulators (DDSMs): deterministic and stochastic. In this two-part paper, a design methodology for reduced-complexity DDSMs is presented. The design methodology is based on error masking. Rules for selecting the word lengths of the stages in multistage architectures are presented. We show that the hardware requirement can be reduced by up to 20% compared with a conventional design, without sacrificing performance. Simulation and experimental results confirm theoretical predictions. Part I addresses MultistAge noise SHaping (MASH) DDSMs; Part II focuses on single-quantizer DDSMs.**

***Index Terms*—Digital delta-sigma modulators (DDSMs), error masking, MultistAge noise SHaping (MASH).**

I. Introduction

DIGITAL DELTA–SIGMA modulators (DDSMs) are often found in consumer communications and entertainment products including cellular telephones, wireless LANs, modems, and MP3 players. The fundamental operation of the DDSM is to quantize an oversampled discrete-amplitude input signal coarsely within a feedback loop such that the power of the resulting quantization noise is shaped within some frequency band of interest. Popular DDSMs are based on two classes of DSMs called MultistAge noise SHaping (MASH) DDSMs and single-quantizer (SQ) DDSMs [1]. MASH DDSMs have a feedforward structure and are inherently stable. SQ DDSMs typically incorporate one or more feedback loops and must be designed with care to ensure stability.

Careful DDSM design is also important because modulator spectrum imperfections directly affect the purity of the output spectrum of the system in which they are used. One of the most challenging issues is the tonal behavior of the DDSM [2]. Often-cited causes of the tonal behavior in a DDSM are the cycles that are particularly likely to occur with slowly varying or dc inputs. The underlying problem is that the randomization of the outputs by the DDSM is often insufficient and the resulting quantization error forms short and repeating patterns (called cycles); this gives rise to strong unwanted tones in the output spectrum [2].

Two classes of techniques have been developed to whiten the quantization noise: deterministic and stochastic. The deterministic approach to whitening the quantization noise is to guarantee maximum cycle lengths by design. Kozak and Kale [3] and, more recently, Borkowski *et al.* [4], [5] have shown that the MASH 111 DDSM does not exhibit large spurs when the input is constant and the initial condition of the first stage is odd, due to the inherent whitening of the quantization error spectrum.

The "stochastic" approach to maximizing cycle lengths is to use a "random"[1] dither signal to disrupt periodic cycles [6]. Dithering breaks up the cycles and increases the effective cycle length, resulting in smooth noise-shaped spectra. Although the stochastic solution inherently adds noise to the spectrum, it is particularly effective when the word length of the DDSM is short, in which case the deterministic technique cannot guarantee a sufficiently long cycle to whiten the quantization error.

In an earlier work [7], we proposed a reduced-complexity (RC) MASH DDSM which maximizes cycle lengths in a deterministic way without dithering. In this paper, we extend this idea, develop the method theoretically, and show how error masking can be used to reduce the hardware consumption (HC) of MASH DDSMs, using either deterministic or stochastic techniques. In Part II, we will focus on SQ DDSMs [8], [14].

In Section II, we review a typical architecture for a MASH DDSM. In Section III, we explain the design methodology for the DDSM using the deterministic technique. In Section IV, a design example for the DDSM using the deterministic technique is shown. In Section V, the design methodology for MASH DDSMs using the stochastic technique is presented. In Section VI, a design example for the stochastic technique is shown. Finally, we draw some conclusions in Section VII.

II. MASH Architectures

Before we explore our design methodology in detail, we first review a conventional MASH DDSM architecture. The structure we consider is based on the digital accumulator model shown in Fig. 1.

In this model, $y[n]$ represents the carry-out signal of a digital accumulator, and the quantizer block Q corresponds to the over-

[1]The dither signal is typically produced by a finite state machine. In this case, it is *pseudorandom* rather than random.

Manuscript received May 12, 2008. First published November 11, 2008; current version published April 10, 2009. This work was supported in part by Science Foundation Ireland under Grants 02/IN1/I045 and 08/IN1/I1854. This paper was recommended by Associate Editor G. Manganaro.

Z. Ye was with the Department of Microelectronic Engineering, Faculty of Engineering, University College Cork, and Tyndall National Institute, Cork, Ireland. He is now with Australian Semiconductor Technology Company (ASTC) Pty Ltd., Adelaide 5000, South Australia (e-mail: zhipeng.ye@astc-design.com).

M. P. Kennedy is with the Department of Microelectronic Engineering, Faculty of Engineering, University College Cork, and Tyndall National Institute, Cork, Ireland (e-mail: peter.kennedy@ucc.ie).

Digital Object Identifier 10.1109/TCSI.2008.2003383

1549-8328/$25.00 © 2009 IEEE

Authorized licensed use limited to: UNIVERSITY COLLEGE CORK. Downloaded on March 26,2010 at 12:10:11 EDT from IEEE Xplore. Restrictions apply.

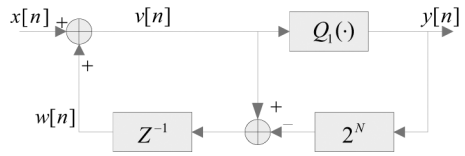

Fig. 1. Digital accumulator model.

flow operation. The signal $v[n]$ is the sum of the digital words $x[n]$ and $w[n]$. When $v[n]$ is greater than 2^N, the quantizer overflows, and the output signal $y[n]$ will be 1 (i.e., truncating quantizer). On the other hand, when $v[n]$ is less than 2^N, the quantizer does not overflow, and $y[n]$ will then be 0. Mathematically, we write

$$y[n] = \begin{cases} 0, & v[n] < 2^N \\ 1, & v[n] \geq 2^N. \end{cases} \tag{1}$$

The function of the digital accumulator is to distribute the power of the quantization error (noise) preferentially toward higher frequencies, thus noise shaping the spectrum.

The effect of the quantizer is usually modeled as an additive quantization noise source e. In the Z-domain, we can write the output $Y(z)$ in terms of $X(z)$ and $E(z)$ as follows:

$$Y(z) = X(z) + (1 - z^{-1})E(z). \tag{2}$$

where X, Y, and E are the z transforms of x,y, and e, respectively.

The output contains not only the input signal but also the quantization error shaped by a filter with transfer function $(1 - z^{-1})$. Ideally, the quantization noise is white and is shaped by the filter so that its power is pushed to the higher frequencies and moved away from the input signal. However, this is not the case for a first-order DDSM. The output signal of the first-order DDSM contains a strong periodic structure, regardless of the output cycle length [9]. A simulation result for a 20-bit first-order DDSM is shown in Fig. 2.

The quantization noise can be whitened and shaped more effectively by a higher order MASH structure. A MASH DDSM uses a cascade of lower order blocks to construct a high-order modulator; it typically comprises first-order modulators or a combination of first- and second-order modulators. The topology of the MASH DDSM is straightforward, and it is stable for all inputs [10]. The simulation result for a 20-bit third-order DDSM is shown in Fig. 3. Note that the power spectrum more closely matches the white-noise approximation in this case and has less tonal behavior. This is because the system has long cycles and the quantization error has been randomized sufficiently.

A. Conventional MASH

The block diagram of an N-bit accumulator of the type shown in Fig. 1 is shown schematically in Fig. 4, where the notation (1, N, N, 1) represents a first order, N-bit input, N-bit quantization error output, and 1-bit carry output, respectively.

Since higher order DSMs are widely used in frequency synthesis applications, we consider, in this paper, the third-order

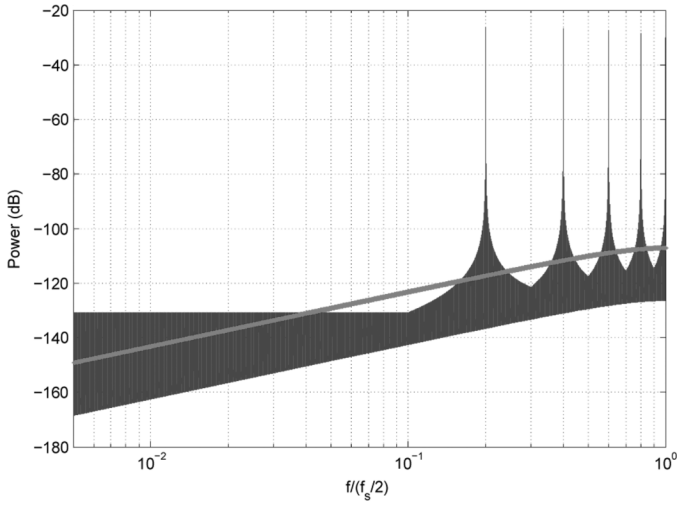

Fig. 2. Simulated power spectrum of a 20-bit first-order DDSM; the input is 104 857. Note the strong tonal behavior resulting from the inadequate whitening of the quantization noise. The smooth curve shows the ideal behavior of the 20-bit first-order DDSM, assuming that the quantization noise is white.

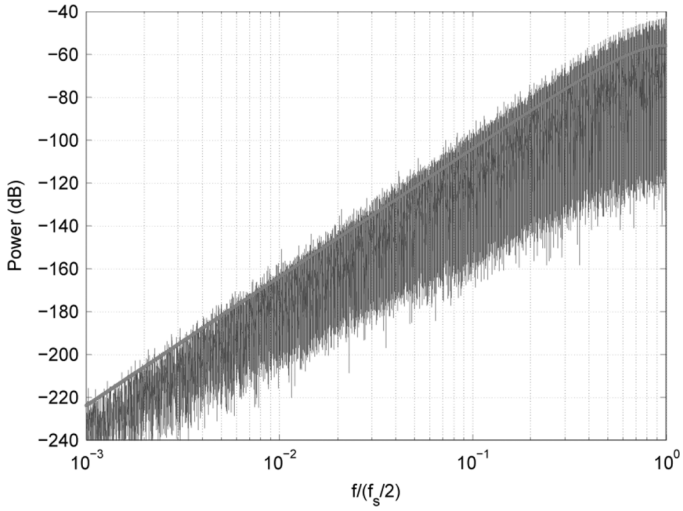

Fig. 3. Simulated power spectrum of a 20-bit third order DDSM; the input is 104 857. The smooth curve shows the ideal behavior of the 20-bit third-order DDSM, assuming that the quantization noise is white.

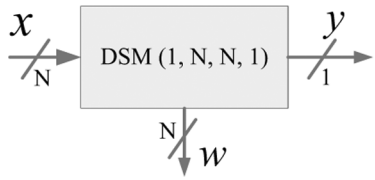

Fig. 4. Block diagram of an N-bit accumulator.

MASH 111 DDSM shown in Fig. 5. This consists of three *identical* N-bit accumulators of the type shown in Fig. 4 and an error cancellation network. MASH 111 indicates that it comprises three first-order accumulators.

The output of the MASH 111 DDSM can be expressed in the Z-domain as

$$Y(z) = STF(z) \cdot X(z) + NTF(z) \cdot E_3(z) \tag{3}$$

Authorized licensed use limited to: UNIVERSITY COLLEGE CORK. Downloaded on March 26,2010 at 12:10:11 EDT from IEEE Xplore. Restrictions apply.

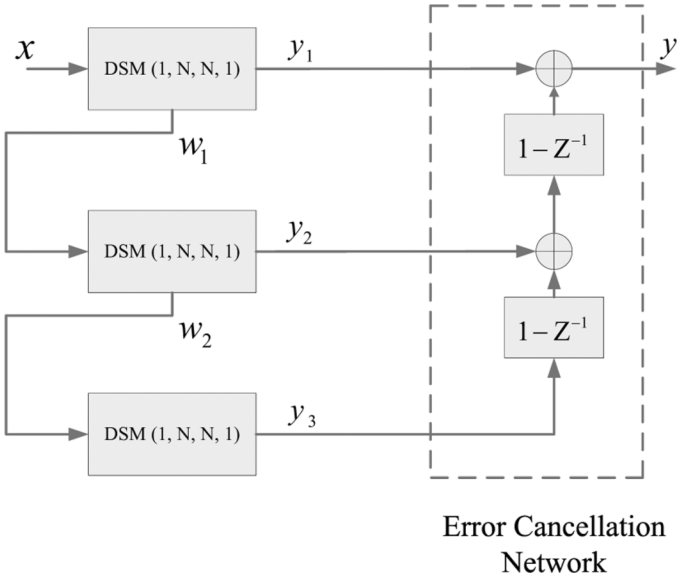

Fig. 5. Block diagram of a MASH 111 DDSM using the accumulator notation of Fig. 4.

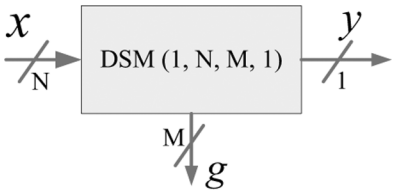

Fig. 6. Block diagram of the N-bit accumulator with an M-bit interstage quantizer.

where $X(z)$, $E_3(z)$, $STF(z)$, and $NTF(z)$ are the z transforms of the input, the quantizer error of the *third* stage, and the signal and noise transfer functions of the modulator, respectively. In this example, $STF(z) = 1$, and the noise transfer function is given by

$$NTF(z) = (1 - z^{-1})^3. \tag{4}$$

Note that the error cancellation network completely removes the quantization errors of the first two stages.

B. RC MASH

In our *RC* MASH DDSM [7], only the first accumulator has a full-width N-bit word. By setting the least significant bit (LSB) of the input to "1", this stage sets the cycle length of the modulator's quantization error to 2^N [5].

The error signal of the first stage passes through an M-bit interstage quantizer Q_M before being fed forward to the next (L-bit) stage. The corresponding block diagram of the first accumulator incorporating an interstage quantizer is shown in Fig. 6.[2] The other accumulators use fewer bits to perform the noise shaping. This allows us to reduce the word lengths in the following stages without reducing the cycle length.

The block diagram of our *RC* MASH 111 DDSM [7], [11] is shown in Fig. 7. The error cancellation network is as in Fig. 5.

[2]The interstage quantization may be realized simply by discarding the $(N - M)$ LSBs.

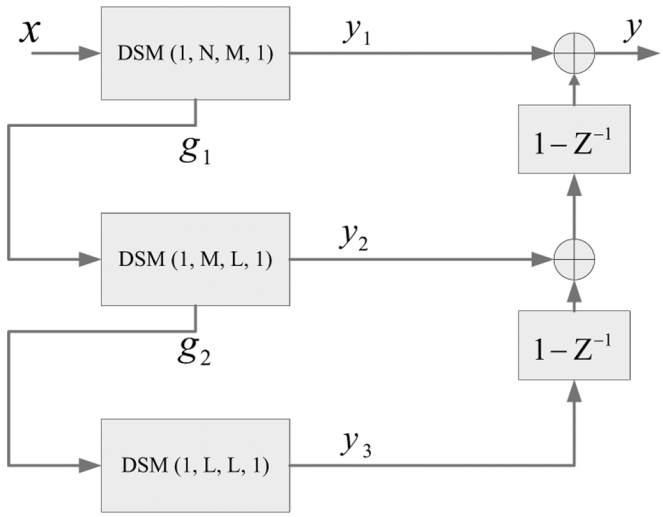

Fig. 7. RC MASH 111 DDSM using the notation of Fig. 6.

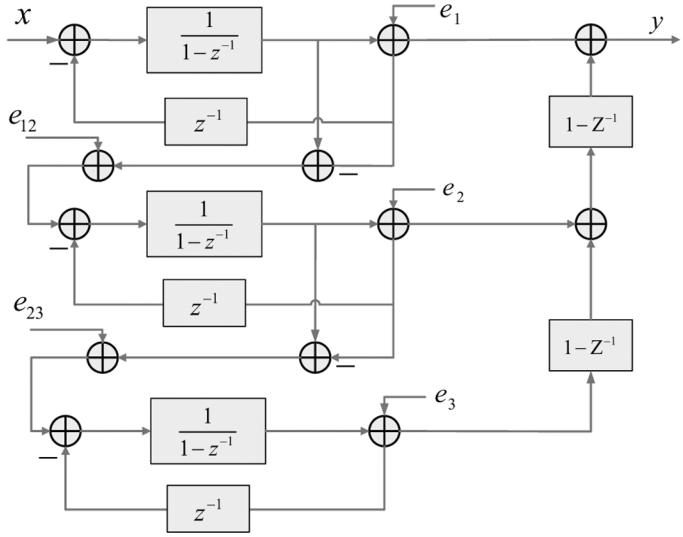

Fig. 8. Linearized model of the *RC* DDSM shown in Fig. 7.

In this case, it does not remove the quantization errors completely, as we will show.

A linearized model which illustrates all the quantization error sources is shown in Fig. 8; its output can be expressed in the Z-domain as

$$Y(z) = STF(z) \cdot X(z) + NTF(z) \cdot E_3(z) + z^{-1}(1 - z^{-1}) \cdot E_{12}(z) + (1 - z^{-1})^2 \cdot E_{23}(z) \tag{5}$$

where $STF(z)$ and $NTF(z)$ are the signal and noise transfer functions, as before. $E_3(z)$ is the z transform of the error introduced by the 1-bit quantizer in the third stage. $E_{12}(z)$ and $E_{23}(z)$ are the z transforms of the quantizer errors introduced by the M- and L-bit interstage quantizers between the first and second and second and third accumulators, respectively.

Note that (5) differs qualitatively from (3) in that it contains two additional shaped noise terms resulting from the errors introduced by the interstage quantizers. By choosing the values of M and L appropriately, these contributions can be masked spectrally by the shaped E_3 term. The guidelines for choosing M and L are presented in Section III.

Authorized licensed use limited to: UNIVERSITY COLLEGE CORK. Downloaded on March 26,2010 at 12:10:11 EDT from IEEE Xplore. Restrictions apply.

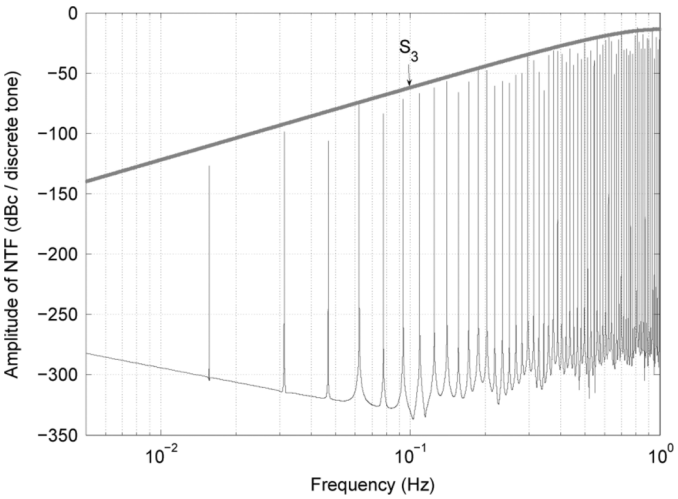

Fig. 9. Power spectrum of a third-order 6-bit MASH DDSM; the input is 7. The DDSM has the structure shown in Fig. 5. The cycle length is 2^7. The smooth curve S_3 is an estimate of the power spectrum obtained by assuming that the quantization noise is white.

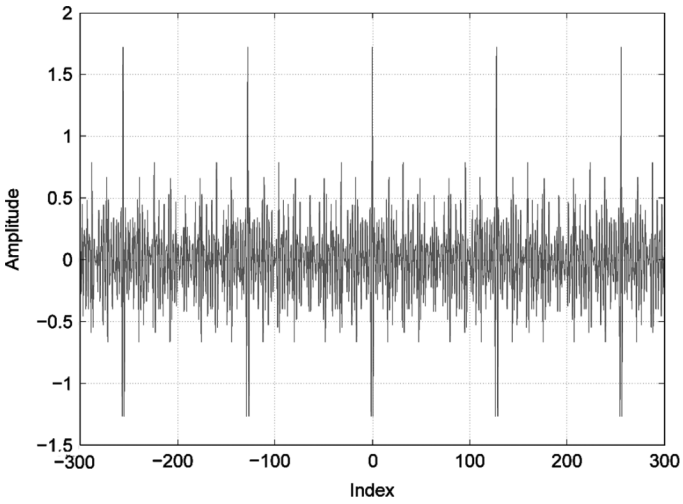

Fig. 10. Autocorrelation result for the third-order 6-bit DDSM; the input is 7.

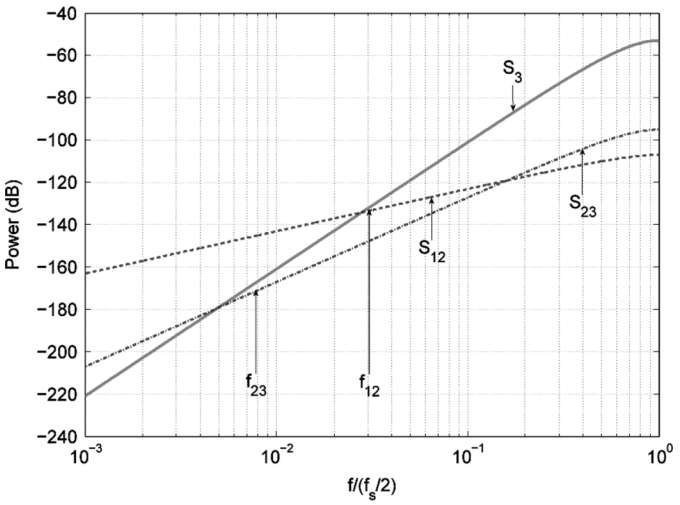

Fig. 11. Masking (dashed) S_{12} and (dotted) S_{23} below (solid) S_3. The lowest frequency tone in N_{23} is at $f_{23}(= f_s/2^{N-L})$; the lowest frequency tone in N_{12} is at $f_{12}(= f_s/2^{N-M})$.

III. Design Methodology (Ditherless Case)

A. Cycle Length and Tone Location of the DDSM

The guaranteed minimum cycle lengths for MASH DDSMs with identical first-order stages have been found empirically by extensive simulation [4] and proven theoretically [5]. For first-, second- and third-order DSMs, the results are 2^N, 2^{N-1}, and 2^{N+1}, respectively, where N is the word length of the accumulator in the DSM, provided that the input is odd in the first-order DDSM and the initial condition is odd in the case of the second- and third-order DDSMs [4], [5].

The quantization noise power is spread over a number of tones that is determined by the cycle length, resulting in a tone spacing of $\Delta f = (f_s)/(L_s)$, where f_s is the sampling frequency and L_s is the cycle length. If Δf is less than the resolution bandwidth of the measuring equipment, the resulting discrete spectrum is indistinguishable experimentally from a continuous spectrum [4]. However, when the cycle length of a DDSM output is not sufficiently large, one can observe discrete tones clearly in the power spectrum. The locations of these tones are given by

$$f[k] = k\Delta f, \qquad k = 1, 2, \ldots, \frac{L_s}{2} \tag{6}$$

where k is the index of the tone.

Fig. 9 shows the output power spectrum of a third-order 6-bit DDSM whose output cycle length L_s is 2^7; this is confirmed by the autocorrelation in Fig. 10, which is periodic with period 128. The discrete power spectrum $P[k]$ of the output y of the DDSM shown in Fig. 9 is defined by

$$P[k] = |Y[k]|^2 \tag{7}$$

where $Y[k]$ is the discrete-time Fourier series [12] of the output of the DDSM with its dc term removed.[3]

[3]In this work, we remove the dc component of the output for illustrative purposes as we are concerned primarily with the spectrum of the quantization noise contribution.

Note that the power spectrum of the shaped quantization noise $NTF(z)E_3(z)$ contains 2^7 discrete tones, as predicted; these are located at $(kf_s)/(2^7)$, with $k = 1, 2, \ldots, 2^7/2$. In particular, the lowest frequency tone appears at $(f_s)/(2^7)$. Note that the x axis is normalized to $f_s/2$ in Fig. 9.

Assuming a cycle of length L_s and additive uniformly distributed white quantization noise, the idealized power spectrum of the shaped noise $NTF(z) \cdot E_3(z)$ is given by

$$S_3(f[k]) = \frac{1}{12L_s} |NTF(z)|^2_{z=e^{j2\pi k/L_s}}, \qquad k = 1, 2, \ldots, \frac{L_s}{2}. \tag{8}$$

Throughout this paper, we will use the power spectrum S_i, which is obtained by assuming that the quantization noise E_i is white, to estimate the power spectrum of the actual shaped quantization noise component N_i.

B. Additional Noise Contributions of the Interstage Quantizers

For notational convenience, let us rewrite (5) as follows:

$$Y(z) = STF(z)X(z) + N_3(z) + N_{12}(z) + N_{23}(z) \tag{9}$$

Authorized licensed use limited to: UNIVERSITY COLLEGE CORK. Downloaded on March 26,2010 at 12:10:11 EDT from IEEE Xplore. Restrictions apply.

where $N_3(z) = NTF(z) \cdot E_3(z)$ is the shaped contribution from the quantizer in the third accumulator, $N_{12}(z) = z^{-1}(1 - z^{-1})E_{12}(z)$ is the shaped contribution of the first interstage quantizer error, and $N_{23}(z) = (1 - z^{-1})^2 E_{23}(z)$ is the shaped contribution of the second interstage quantizer error.

Assuming that all quantization noise terms can be modeled by independent white sources, we estimate the power spectrum of $N_3(z)$ as

$$S_3(f[k]) = \frac{1}{12L_s}\left|(1-z^{-1})^3\right|^2_{z=e^{j2\pi k/L_s}} \tag{10}$$

where L_s is the cycle length.

In the same manner, the spectra obtained by assuming white error sources e_{12} and e_{23} are given by

$$S_{12}(f[k]) = \frac{\Delta_{12}^2}{12L_{12}}\left|z^{-1}(1-z^{-1})\right|^2_{z=e^{j2\pi k/L_{12}}} \tag{11}$$

$$S_{23}(f[k]) = \frac{\Delta_{23}^2}{12L_{23}}\left|(1-z^{-1})^2\right|^2_{z=e^{j2\pi k/L_{23}}} \tag{12}$$

where Δ_{12} and Δ_{23} are the quantization steps of the M- and L-bit interstage quantizers, which are $(1)/(2^M)$ and $(1)/(2^L)$, respectively. We denote by L_{12} and L_{23} the cycle lengths (periods) of the error signals from the interstage quantizers. We will show in the following how these lengths can be determined.

Let us express the dc input X to the DDSM in binary form, which is $x_N, x_{N-1}, \ldots, x_1$, and separate it into its upper and lower pieces as follows:

$$\begin{aligned}&\{x_N, x_{N-1}, \ldots, x_1\}\\ &\quad = X_{\text{upper}} + X_{\text{lower}}\\ &\quad = \{x_N, x_{N-1}, \ldots, x_{N-M+1}, 0_{N-M}, \ldots, 0_1\}\\ &\qquad + \{0_N, 0_{N-1}, \ldots, 0_{N-M+1}, x_{N-M}, x_{N-M-1}, \ldots, x_1\}.\end{aligned} \tag{13}$$

Since the $(N - M)$ LSBs of X_{upper} are 0, they do not contribute to N_{12}. Therefore, X_{lower} alone determines N_{12}. Since the M most significant bits are 0, the error output for X_{lower} feeding through the N-bit accumulator is the same as that feeding through an $(N - M)$-bit accumulator. Consequently, the cycle length of N_{12} is the same as the output cycle length of an $(N - M)$-bit word feeding through an $(N - M)$-bit accumulator. If we set the LSB of the input to "1," the cycle length L_{12} in this case is 2^{N-M} [5]. In the same manner, the cycle length L_{23} for N_{23} is 2^{N-L}. Thus

$$\begin{aligned}L_3 &= 2^N\\ L_{12} &= 2^{N-M}\\ L_{23} &= 2^{N-L}.\end{aligned} \tag{14}$$

The correlation function γ, shown in the following equation, can be used to quantify the interdependencies of N_{12}, N_{23}, and N_3:

$$\gamma = \frac{N\Sigma xy - (\Sigma x)(\Sigma y)}{\sqrt{[N\Sigma x^2 - (\Sigma x)^2][N\Sigma y^2 - (\Sigma y)^2]}}. \tag{15}$$

We have performed extensive simulations for different combinations of N, M, and L, and the correlation results are below 0.02 in each case. Therefore, we conclude empirically that N_{12}, N_{23}, and N_3 can be made almost independent of each other.

By *assuming* independence, the noise power spectrum at the output of the *RC* MASH DDSM can be approximated by

$$\begin{aligned}S(f[k]) &= S_3(f[k]) + S_{12}(f[k]) + S_{23}(f[k])\\ &= \frac{1}{12L_s}\left|(1-z^{-1})^3\right|^2_{z=e^{j2\pi k/L_s}}\\ &\quad + \frac{\Delta_{12}^2}{12L_{12}}\left|z^{-1}(1-z^{-1})\right|^2_{z=e^{j2\pi k/L_{12}}}\\ &\quad + \frac{\Delta_{23}^2}{12L_{23}}\left|(1-z^{-1})^2\right|^2_{z=e^{j2\pi k/L_{23}}},\\ &\qquad k = 1, 2, \ldots, \frac{L_s}{2}.\end{aligned} \tag{16}$$

C. Error Masking Strategy

The idea of our word-length selection strategy [11] is to mask the contributions of the intermediate quantizers by hiding the noise components N_{12} and N_{23} below the N_3 component.

The idea is shown graphically in Fig. 11. The spectral envelopes S_{12} and S_{23} due to the interstage quantizers should lie below the S_3 envelope. Since all are discrete spectra, the constraints apply at a finite number of points.

In particular, we require that

$$S_{12} < S_3@f = f_s \cdot k/L_{12}, \qquad k = 1, 2, \ldots, L_{12}/2 \tag{17}$$

$$S_{23} < S_3@f = f_s \cdot k/L_{23}, \qquad k = 1, 2, \ldots, L_{23}/2. \tag{18}$$

Recall that, for a DSM with an output cycle length of L_s, the lowest frequency tone is at f_s/L_s. Therefore, since the cycle lengths for N_{12} and N_{23} are 2^{N-M} and 2^{N-L}, the lowest frequency tones in the power spectra of N_{12} and N_{23} are at $f_s/2^{N-M}$ and $f_s/2^{N-L}$, respectively.

Additionally, at the output of the *RC* DDSM, since S_{12} and S_{23} are first- and second-order shaped, respectively, while S_3 is third-order shaped, if the levels of the lowest frequency tones in N_{12} and N_{23} are below that of N_3, the overall power of N_{12} and N_{23} should always be below the S_3 envelope. Based on this idea, the constraints can be rewritten as

$$S_{12} < S_3@f = f_s/2^{N-M} \tag{19}$$

$$S_{23} < S_3@f = f_s/2^{N-L}. \tag{20}$$

Since

$$\begin{aligned}|1 - z^{-1}|^2 &= |1 - e^{-j2\pi f/f_s}|^2\\ &= |2\sin(\pi f/f_s)|^2\end{aligned} \tag{21}$$

$$\sin(\pi f/f_s) \approx \pi f/f_s \qquad \text{for } f \ll f_s \tag{22}$$

we can approximate S_{12}, S_{23}, and S_3 at low frequencies by

$$S_{12} \approx \frac{\Delta_{12}^2}{12L_{12}} \cdot 2^2(\pi f/f_s)^2 \tag{23}$$

$$S_{23} \approx \frac{\Delta_{23}^2}{12L_{23}} \cdot 2^4(\pi f/f_s)^4 \tag{24}$$

$$S_3 \approx \frac{1}{12L_3} \cdot 2^6(\pi f/f_s)^6. \tag{25}$$

Substituting (23), (24), and (25) into the constraints (19) and (20), we obtain

$$\frac{1}{2^{2M}} \cdot \frac{1}{12 \cdot 2^{N-M}} \cdot 2^2 \cdot \frac{\pi^2}{(2^{N-M})^2} < \frac{1}{12 \cdot 2^N} \frac{2^6\pi^6}{(2^{N-M})^6} \tag{26}$$

Authorized licensed use limited to: UNIVERSITY COLLEGE CORK. Downloaded on March 26,2010 at 12:10:11 EDT from IEEE Xplore. Restrictions apply.

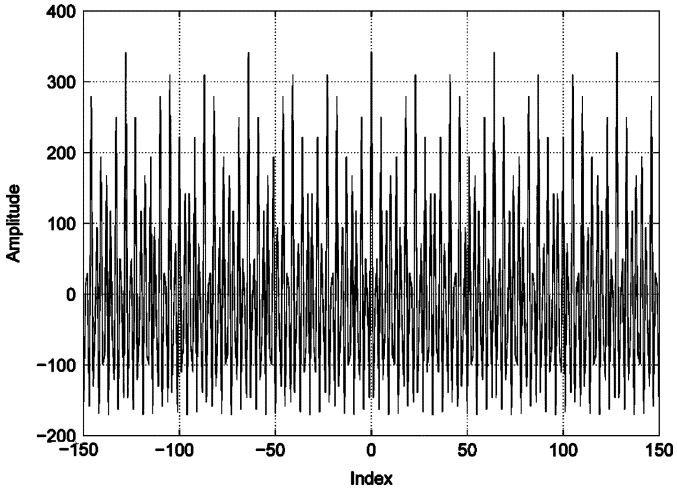

Fig. 12. Autocorrelation result for N_{12} in a 20–14–12 MASH DDSM when the input is 104 857. The cycle length is $2^6 (= 64)$.

$$\frac{1}{2^{2L}} \cdot \frac{1}{12 \cdot 2^{N-L}} \cdot 2^4 \cdot \frac{\pi^4}{(2^{N-L})^4} < \frac{1}{12 \cdot 2^N} \frac{2^6 \pi^6}{(2^{N-L})^6} \quad (27)$$

which reduce to

$$4N - 5M - 4 < 4 \log_2(\pi) \approx 6.6 \quad (28)$$

$$2N - 3L - 2 < 2 \log_2(\pi) \approx 3.3. \quad (29)$$

Based on (28) and (29), in order to design an *RC* $N-M-L$ MASH DDSM with the same cycle length and similar power spectrum as a conventional N_0-bit MASH DDSM, the design procedure is as follows.

1) Choose $N = N_0 + 1$ to ensure that the output cycle length of the *RC* MASH DDSM is the same as that of the conventional N_0-bit MASH DDSM.
2) Choose $M = \text{ceil}((4N - 10.6)/(5))$ [from (28)] to ensure that the power of the first tone of N_{12} is less than S_3 at the frequency $f_s/2^{N-M}$, where $\text{ceil}(x)$ means the smallest integer greater than x.
3) Choose $L = \text{ceil}((2N - 5.3)3)$ [from (29)] to ensure that the power of the first tone of N_{23} is less than S_3 at the frequency $f_s/2^{N-L}$.

D. Hardware Requirements

Since the accumulators consume most of the hardware in the DDSM and the HC of the accumulators is proportional to their word lengths, we can estimate the relative HC (RHC) of our *RC* MASH DDSM compared with the conventional MASH DDSM as

$$RHC \approx N_0 + \text{ceil}\left(\frac{4N_0 - 6.6}{5}\right) + \text{ceil}\left(\frac{2N_0 - 3.3}{3}\right) 3N_0$$
$$\approx \frac{2.47N_0 - 1.42}{3N_0} \times 100\% \quad (30)$$

where the word length of the reference MASH DDSM is N_0, and we choose N, M, and L as in Section III.C. Asymptotically, RHC approaches 82% for large N_0's. When $N_0 = 19$, (30) predicts that our *RC* implementation will require 20% less hardware than a conventional implementation with identical accumulators.

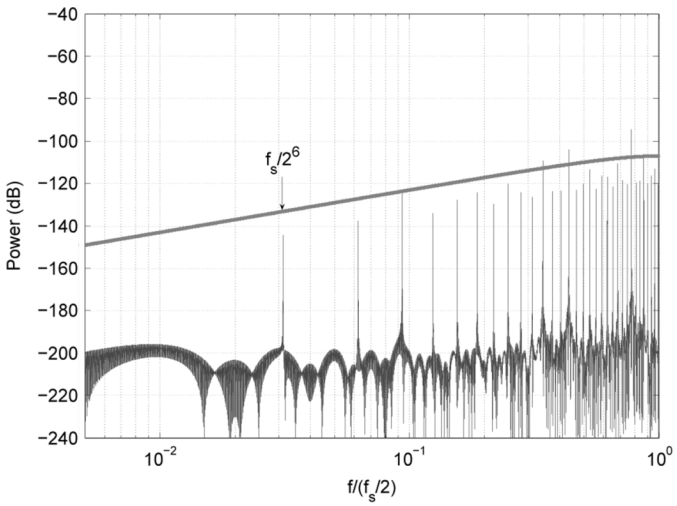

Fig. 13. Simulated power spectrum for N_{12} when $N = 20$, $M = 14$, and $L = 12$; the input is 104 857. The first spur is at $f_s/2^6$. The smooth curve is $S_{12}(11)$.

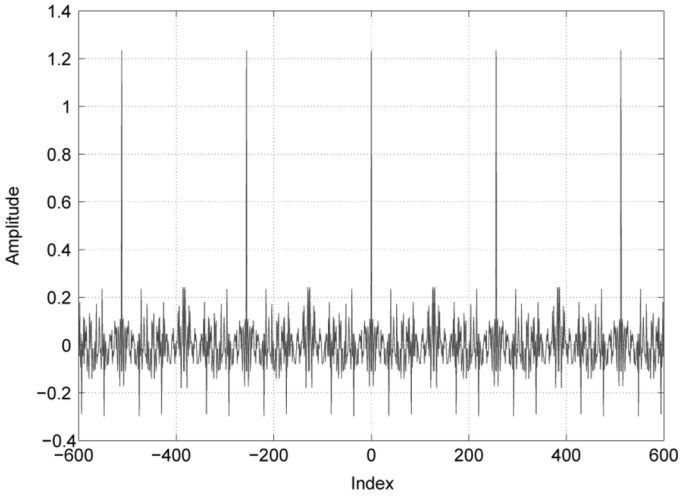

Fig. 14. Autocorrelation result for N_{23}; the input is 104 857. The cycle length is 256.

IV. Design Example

In order to verify the design methodology in Section III.C, we present a design example for a 19-bit MASH DDSM. The optimum word lengths of the first, second, and third stages of the *RC* MASH DDSM are 20, 14, and 12, respectively.

First, we simulate the 20–14–12 *RC* MASH DDSM to show typical contributions N_{12},N_{23}, and N_3. In Fig. 12, the autocorrelation result confirms that the cycle length of N_{12} is 2^6. Fig. 13 shows the power spectrum of N_{12}. The power spectrum S_{12} based on the white-noise approximation (11) is overlaid as well. As expected, the quantization powers are spread over $2^{20-14} = 2^6$ discrete tones, while the location and power of the lowest frequency tone are $f_s/2^6$ and approximately -146 dB, respectively. In addition, N_{12} is shaped by 20 dB/dec, which is the same as for a first-order DDSM.

In Fig. 14, the autocorrelation calculation confirms that the cycle length of N_{23} is $2^8 (= 256)$. Fig. 15 shows the simulated

Authorized licensed use limited to: UNIVERSITY COLLEGE CORK. Downloaded on March 26,2010 at 12:10:11 EDT from IEEE Xplore. Restrictions apply.

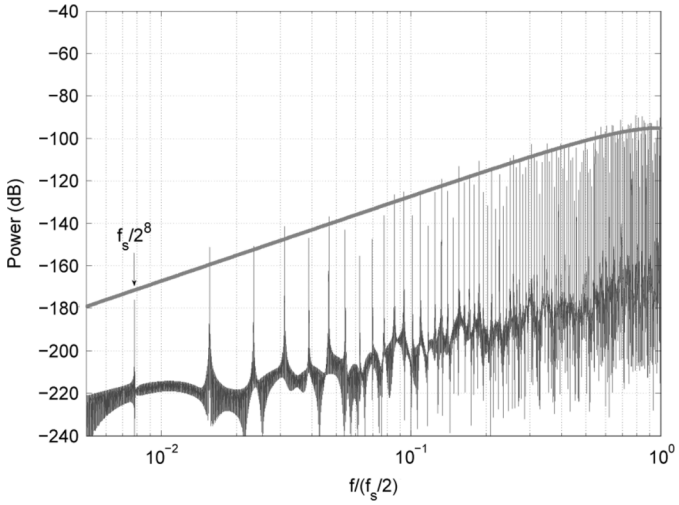

Fig. 15. Simulated power spectrum for N_{23} when $N = 20$, $M = 14$, and $L = 12$; the input is 104 857. The first spur is at $f_s/2^8$. The smooth curve is $S_{23}(12)$.

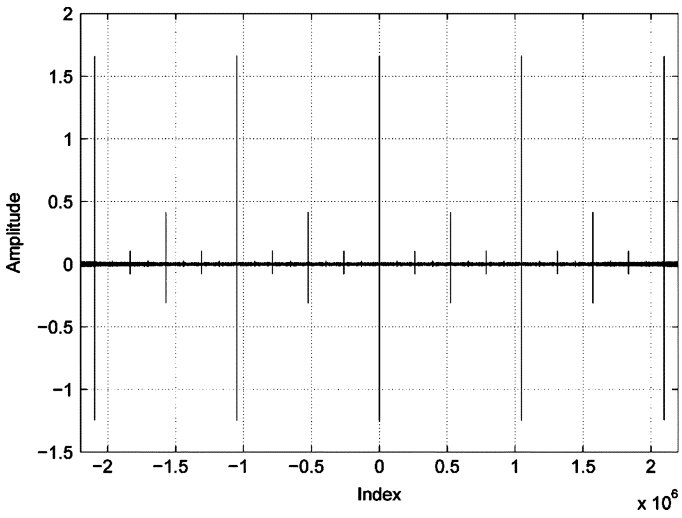

Fig. 16. Autocorrelation result for N_3; the input is 104 857. The cycle length is 1 048 576.

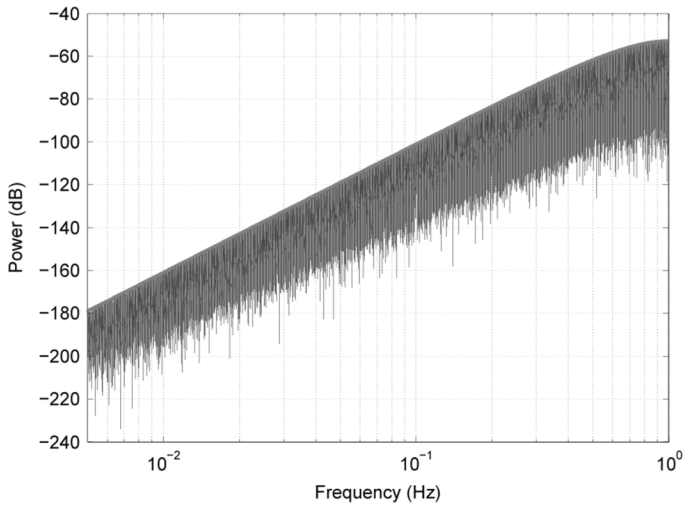

Fig. 17. Simulated power spectrum for N_3 when $N = 20$, $M = 14$, and $L = 12$; the input is 104 857. The smooth curve is $S_3(10)$.

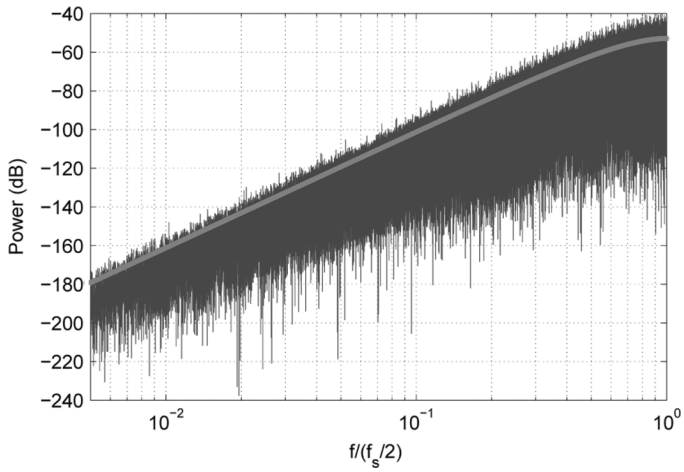

Fig. 18. Simulated output power spectrum for a conventional 19-bit MASH 111 DDSM; the input is 52 429. The dc term has been removed. The smooth curve is $S_3(10)$.

output power spectrum N_{23} with the overlaid white-noise prediction $S_{23}(12)$, from which we can see that N_{23} is shaped by 40 dB/dec, as expected. The lowest frequency tone is located at $f_s/2^{20-12}(= f_s/2^8)$, at approximately -178 dB.

In Fig. 16, the autocorrelation result for N_3 confirms that the cycle length is $2^{20}(= 1\,048\,576)$. Fig. 17 shows the simulated power spectrum for N_3 and the white-noise estimate S_3.

A. Simulations

To compare the conventional and *RC* modulators, we present simulation results. The inputs of the DDSM are selected as the odd numbers that set the normalized input as close as possible to the value 0.1, i.e., $X = 104\,857$ in this case. The simulated output power spectrum of the conventional 19-bit MASH DDSM is shown in Fig. 18. Its cycle length of 2^{20} is confirmed by Fig. 19.

The output power spectrum for the 20–14–12 *RC* MASH DDSM is shown in Fig. 20. Note that the N_{12} and N_{23} components lie below the spectral envelope of N_3 and are therefore masked by it, as expected. Consequently, N_{12} and N_{23} do not adversely affect the overall performance of the DDSM. On the contrary, the additional quantization error sources serve to whiten the error, resulting in a smoother spectrum overall.

The cycle length of 2^{20} is confirmed by Fig. 21.

B. Experimental Results

We constructed an experimental demonstration system on a Xilinx Spartan-2E field-programmable-gate-array board clocked at $f_s = 1.67$ MHz. The modulator output was converted to continuous time using an Analog Devices AD5445 12-bit DAC with a zeroth-order hold and a low-pass filter with a bandwidth of 10 MHz. Spectral measurements were made using an Agilent E4402B Spectrum Analyzer.

Experimental measurements of the power spectrum of the conventional 19-bit MASH DDSM are shown in Fig. 22.

Note that the power spectrum of the conventional 19-bit MASH DDSM is relatively spiky compared to that in the *RC*

Authorized licensed use limited to: UNIVERSITY COLLEGE CORK. Downloaded on March 26,2010 at 12:10:11 EDT from IEEE Xplore. Restrictions apply.

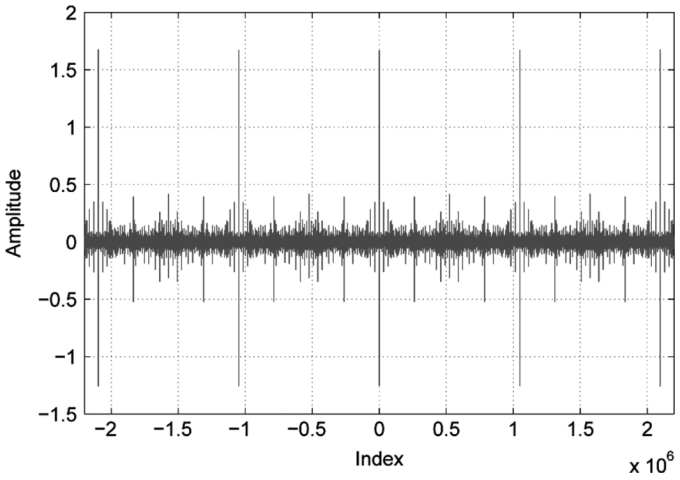

Fig. 19. Autocorrelation result for a conventional 19-bit MASH DDSM; the input is 52 429.

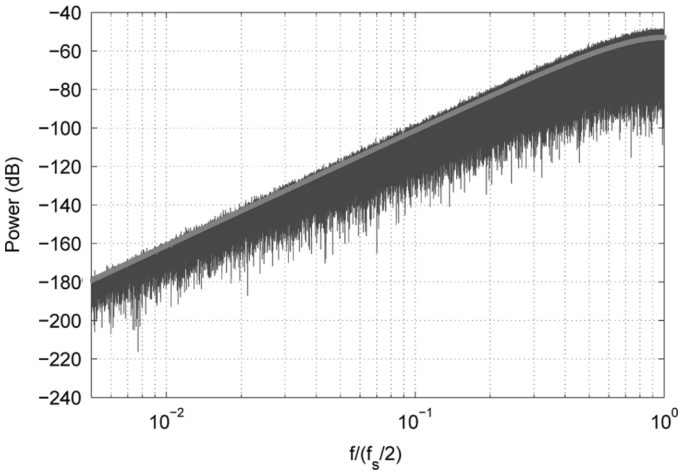

Fig. 20. Simulated output power spectrum for an *RC* 20–14–12-bit MASH 111 DDSM; the input is 104 857. The dc term has been removed. The smooth curve is $S_3(10)$ (Compare with Fig. 18).

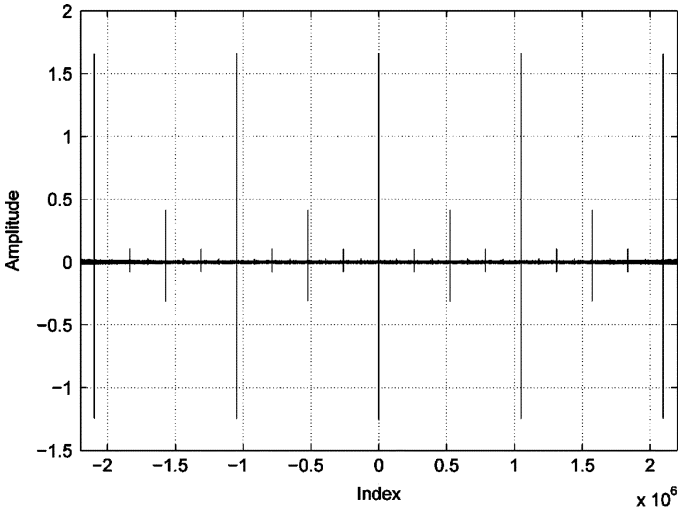

Fig. 21. Autocorrelation result for *RC* MASH DDSM when $N = 20$, $M = 14$, and $L = 12$; input is 104 857. The cycle length is 2^{20}.

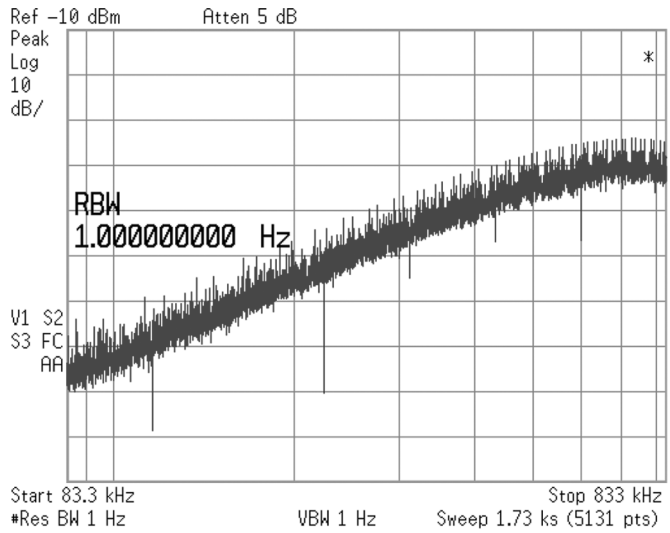

Fig. 22. Measured power spectrum of the output of a 19-bit MASH 111 DSM; the input is 52 429.

case, due to the poorer whitening of the quantization noise, as shown in Fig. 19.

Experimental measurements of the power spectrum of the 20–14–12 MASH modulator are shown in Fig. 23. As expected, the noise is shaped at 60 dB/dec. Moreover, the spectrum of the new structure is smoother, as expected, due to the more effective whitening of the quantization noise spectrum, as shown in Fig. 21.

The spectrum of the new structure is smoother and closer to the ideal, even with the same cycle length as the conventional DDSM, due to the more effective whitening of the quantization noise spectrum.

C. HC

The hardware requirements for 1) a conventional 19-bit MASH 111 DDSM and 2) the 20–14–12-bit *RC* DDSM without dither are summarized in Table I. The HC is reported as the number of flip-flops and the number of four-input lookup tables which represent the synchronous and the asynchronous logic, respectively. The total-equivalent-gate (TEG) count for the design is given as well. These results are based on the map report from the Xilinx ISE program [13]; a full custom implementation could potentially do better.

The 20–14–12 *RC* MASH DDSM has a marginally better spectral performance than the 19-bit conventional MASH DDSM, with 20% less hardware (TEG); this agrees with our prediction (30).

V. Design Methodology (with Dither)

A. Additional Noise Contributions of the Interstage Quantizers

In the case of additive input dithering of a MASH system [6], a *1-bit dither* pseudorandom signal d filtered by a shaping filter $V(z)$ is added to the LSBs of a *desired signal* x as shown in Fig. 24.

With dithering, the minimum cycle length of the DDSM is guaranteed to be at least as large as that of the dither generator. This can be significantly larger than the cycle length in a ditherless DDSM. Consequently, the tone spacing is typically

Authorized licensed use limited to: UNIVERSITY COLLEGE CORK. Downloaded on March 26,2010 at 12:10:11 EDT from IEEE Xplore. Restrictions apply.

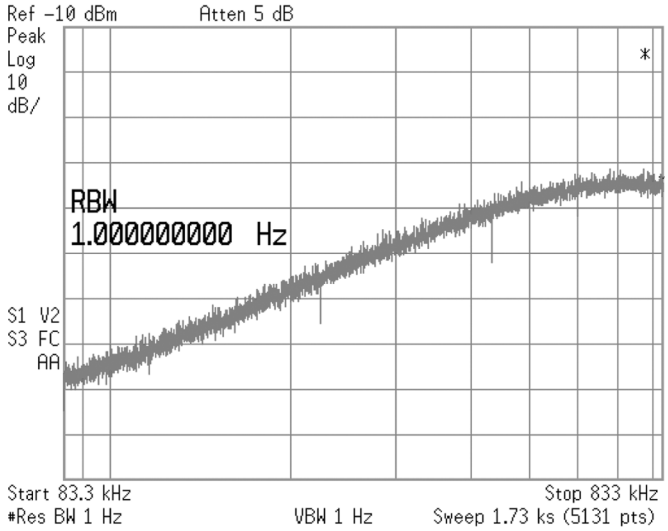

Fig. 23. Measured power spectrum of the output of the *RC* MASH DDSM when $N = 20$, $M = 14$, and $L = 12$; the input is 104 857.

TABLE I
HC OF THE CONVENTIONAL 19-BIT MASH 111 DDSM AND THE 20–14–12-BIT *RC* DDSM WITHOUT DITHER SYNTHESIZED USING XILINX ISE

MASH DDSM	Hardware Consumption		
	FFs	LUTs	TEGs
(a) 19 bit	113	68	1579
(b) 20-14-12 bit	90	57	1263
((b)/(a))%	79.6%	83.8%	80%

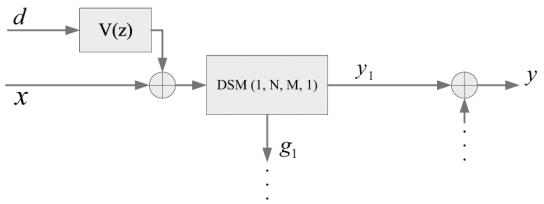

Fig. 24. LSB dithering in MASH DDSM.

very small. When the tones are spaced sufficiently closely, the discrete spectrum tends toward a continuous spectrum. In this case, the discrete power spectrum representation can be approximated by a power spectral density (PSD) $\mathcal{L}$ expressed in units of decibels relative to the carrier per hertz [4]. By convention [4], $\mathcal{L}$ can be determined by summing the discrete tones of $P[k]$ that fall into the ith bin with bandwidth BW. Thus

$$\mathcal{L}(i \cdot BW) = \frac{1}{BW} \sum_{(i-1)\cdot BW < \omega_k \le i \cdot BW} P[k]. \tag{31}$$

The phase noise $\mathcal{L}(i \cdot BW)$ can be estimated using the traditional linear model, assuming white quantization noise [1]

$$\mathcal{L}(f) = \frac{\Delta^2}{12} |NTF|^2. \tag{32}$$

Comparing with (10), (11), and (12), the PSDs of the filtered error signals N_3, N_{12}, and N_{23} can respectively be expressed as

$$\mathcal{L}_3(f) = \frac{1}{12} \left|(1 - z^{-1})^3\right|^2_{z=e^{j2\pi f}} \tag{33}$$

$$\mathcal{L}_{12}(f) = \frac{\Delta_{12}^2}{12} \left|z^{-1}(1 - z^{-1})\right|^2_{z=e^{j2\pi f}} \tag{34}$$

$$\mathcal{L}_{23}(f) = \frac{\Delta_{23}^2}{12} \left|(1 - z^{-1})^2\right|^2_{z=e^{j2\pi f}}. \tag{35}$$

By once again *assuming* independence, the PSD of the error signal at the output of the dithered *RC* MASH DDSM can be expressed as

$$\mathcal{L}(f) = \mathcal{L}_3(f) + \mathcal{L}_{12}(f) + \mathcal{L}_{23}(f) + \mathcal{L}_{\rm nf}(f) \tag{36}$$

where $\mathcal{L}_{\rm nf}(f)$ is the contribution due to the dither signal, and we have assumed that $STF(z) = 1$.

B. Zeroth-Order Dither

Because of dithering, the cycle lengths of e_{12} and e_{23} are so long that it is hard to find the locations of their *first tones*. Therefore, (19) and (20) cannot be used as constraints to select the DDSM word lengths. Nevertheless, we can still mask the N_{12} and N_{23} components below N_3.

It can be shown that, for a DDSM with dithering, the low-frequency noise floor is typically dominated by the dither signal. In the case of a zeroth-order shaped dither, the level of the noise floor is

$$\mathcal{L}_{\rm nf0} = \frac{1}{12 \cdot (2^N)^2}. \tag{37}$$

In this case, we need to hide the components N_{12} and N_{23} below the contributions of N_3 and the noise floor $\mathcal{L}_{\rm nf}$. The largest frequency at which the PSD of the dithering is larger than the contribution from e_3 can be calculated as

$$\frac{1}{12} \left|(2\sin(\pi f_0/f_s))\right|^6 = \frac{1}{12 \cdot 2^{2N}}. \tag{38}$$

Assuming

$$\sin(\pi f_0/f_s) \approx \pi f_0/f_s \qquad \text{for } f_0 \ll f_s \tag{39}$$

as before results in

$$f_0 = \frac{1}{\pi \cdot 2^{N/3}} \cdot \frac{f_s}{2} \tag{40}$$

for a sufficiently large N. Therefore, we apply the following constraints: $\mathcal{L}_{12} < \mathcal{L}_{\rm nf}$ and $\mathcal{L}_{23} < \mathcal{L}_{\rm nf}$ for $f < f_0$, and $\mathcal{L}_{12} < \mathcal{L}_3$ and $\mathcal{L}_{23} < \mathcal{L}_3$ for $f > f_0$.

As $\mathcal{L}_{12}$ and $\mathcal{L}_{23}$ are first- and second-order shaped, respectively, $\mathcal{L}_{12} < \mathcal{L}_3$ and $\mathcal{L}_{23} < \mathcal{L}_3$ at f_0 implies that $\mathcal{L}_{12} < \mathcal{L}_3$ and $\mathcal{L}_{23} < \mathcal{L}_3$ for $f > f_0$. Therefore, we need only to check the constraint at the boundary. In particular, the constraints can be written as

$$\mathcal{L}_{12} < \mathcal{L}_3 @ f_0 \tag{41}$$

$$\mathcal{L}_{23} < \mathcal{L}_3 @ f_0 \tag{42}$$

as shown in Fig. 25.

We approximate $\mathcal{L}_{12}$, $\mathcal{L}_{23}$, and $\mathcal{L}_3$ at low frequencies by

$$\mathcal{L}_{12} \approx \frac{\Delta_{12}^2}{12} \cdot 2^2 (\pi f/f_s)^2 \tag{43}$$

$$\mathcal{L}_{23} \approx \frac{\Delta_{23}^2}{12} \cdot 2^4 (\pi f/f_s)^4 \tag{44}$$

Authorized licensed use limited to: UNIVERSITY COLLEGE CORK. Downloaded on March 26,2010 at 12:10:11 EDT from IEEE Xplore. Restrictions apply.

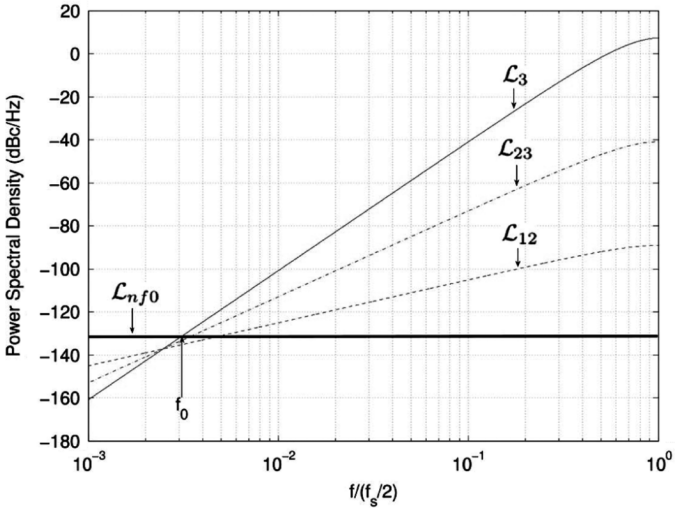

Fig. 25. Masking $\mathcal{L}_{12}$ and $\mathcal{L}_{23}$ below $\mathcal{L}_3$ at f_0.

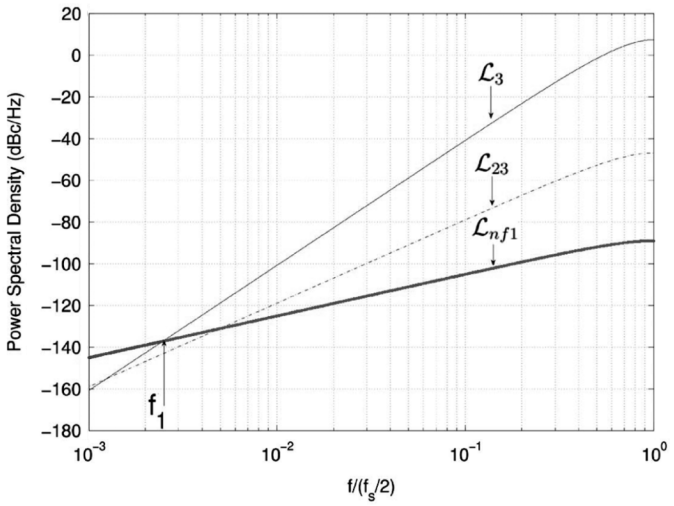

Fig. 26. Masking $\mathcal{L}_{23}$ below $\mathcal{L}_3$ at f_1.

$$\mathcal{L}_3 \approx \frac{1}{12} \cdot 2^6 (\pi f/f_s)^6. \tag{45}$$

Substituting (43), (44), and (45) into the constraints (41) and (42), we obtain

$$\frac{1}{2^{2M}} \cdot \frac{1}{12} \cdot \left(\frac{1}{2^{N/3}}\right)^2 < \frac{1}{12} \cdot \left(\frac{1}{2^{N/3}}\right)^6 \tag{46}$$

$$\frac{1}{2^{2L}} \cdot \frac{1}{12} \cdot \left(\frac{1}{2^{N/3}}\right)^4 < \frac{1}{12} \cdot \left(\frac{1}{2^{N/3}}\right)^6 \tag{47}$$

which reduce to

$$M > \frac{2N}{3} \tag{48}$$

$$L > \frac{N}{3}. \tag{49}$$

Based on (48) and (49), if the word length N of the first stage of the DDSM is determined, the optimum word lengths M and L of the second and third stages can be calculated as

$$M = \text{ceil}\left(\frac{2N}{3}\right) \tag{50}$$

$$L = \text{ceil}\left(\frac{N}{3}\right). \tag{51}$$

C. First-Order Dither

If a first-order shaped dither is applied to the input of the DDSM, its noise floor is defined by

$$\mathcal{L}_{nf1} = \frac{1}{12 \cdot (2^N)^2} \left|(2\sin(\pi f/f_s))\right|^2. \tag{52}$$

The largest frequency at which the PSD of the dither component is larger than that from e_3 can be calculated as

$$\frac{1}{12} \left|(2\sin(\pi f_1/f_s))\right|^4 = \frac{1}{12 \cdot 2^{2N}} \tag{53}$$

which results in

$$f_1 \approx \frac{1}{\pi} \cdot \frac{1}{2^{N/2}} \cdot \frac{f_s}{2}. \tag{54}$$

Since $\mathcal{L}_{12}$ is first-order shaped, just like the dither, we require that $\mathcal{L}_{12} < \mathcal{L}_{\text{nf1}}$, which can be expressed as

$$\frac{\Delta_{12}^2}{12} \cdot 2^2 (\pi f/f_s)^2 \leq \frac{1}{12 \cdot (2^N)^2} \cdot 2^2 (\pi f/f_s)^2 \tag{55}$$

which reduces to

$$M \geq N. \tag{55}$$

Therefore, $M \geq N$. Since our objective is to reduce the overall hardware requirement, we choose $M = N$. Next, $\mathcal{L}_{23}$ needs to be masked by $\mathcal{L}_3$, as shown schematically in Fig. 26.

Thus, the word-length selection strategy for the third accumulator requires that

$$\mathcal{L}_{23} < \mathcal{L}_3 @ f_1. \tag{57}$$

This can be expanded as

$$\frac{1}{2^{2M}} \cdot \frac{1}{12} \cdot \left(\frac{1}{2^{N/2}}\right)^4 < \frac{1}{12} \cdot \left(\frac{1}{2^{N/2}}\right)^6 \tag{58}$$

which gives

$$L > \frac{N}{2}. \tag{59}$$

If we want to ensure that $\mathcal{L}_{23}$ is further below $\mathcal{L}_3$, we can impose a guard band of 3 dB, for example. In this way, we force $\mathcal{L}_{12}$ to be half of $\mathcal{L}_3$ at f_1, and the constraint becomes

$$L > \frac{N+1}{2}. \tag{60}$$

Authorized licensed use limited to: UNIVERSITY COLLEGE CORK. Downloaded on March 26,2010 at 12:10:11 EDT from IEEE Xplore. Restrictions apply.

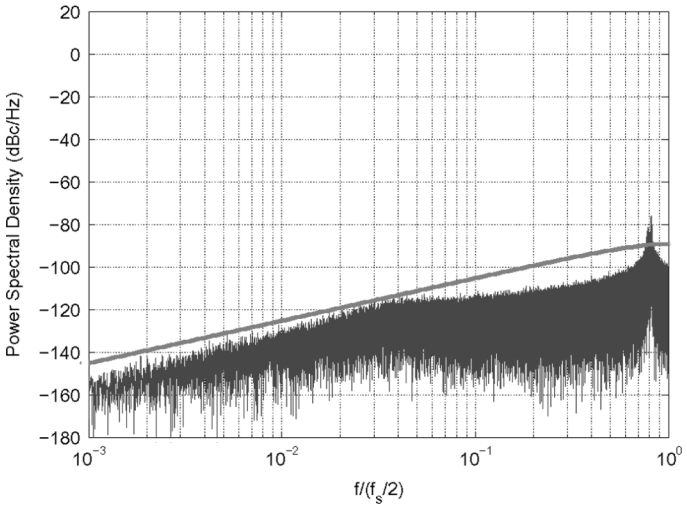

Fig. 27. Simulated PSD for N_{12} when $N = 20$, $M = 14$, and $L = 7$; the input is 104 857. The smooth curve is $\mathcal{L}_{12}(34)$.

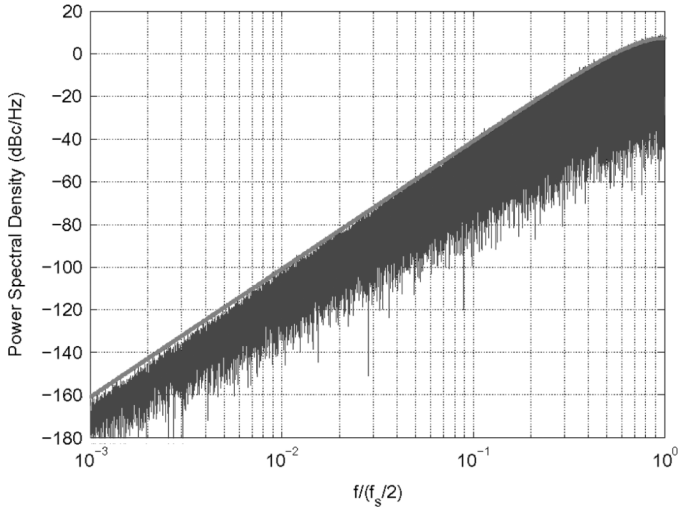

Fig. 29. Simulated PSD for N_3 when $N = 20$, $M = 14$, and $L = 7$; the input is 104 857. The smooth curve is $\mathcal{L}_3(33)$.

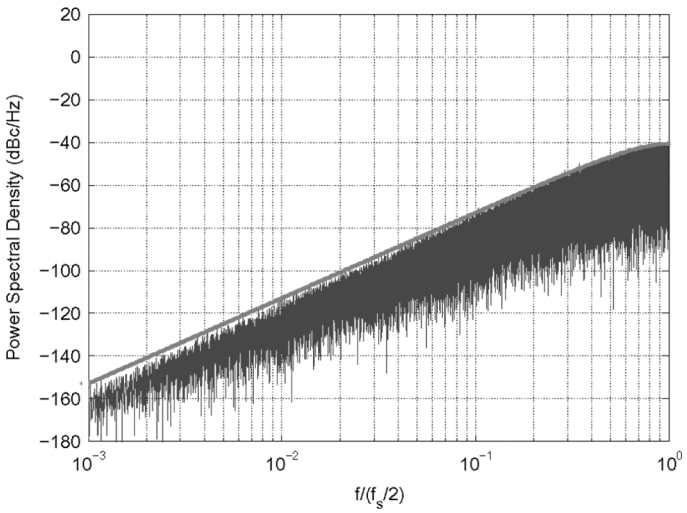

Fig. 28. Simulated PSD for N_{23} when $N = 20$, $M = 14$, and $L = 7$; the input is 104 857. The smooth curve is $\mathcal{L}_{23}(35)$.

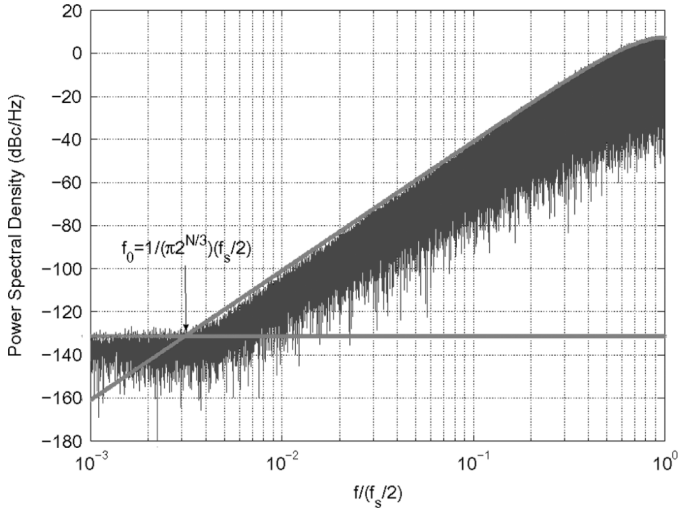

Fig. 30. Simulated PSD at the output of a zeroth-order dithered 20-bit MASH 111 DDSM; the input is 104 857. The dc term has been removed. The solid curves are $\mathcal{L}_3$ and $\mathcal{L}_{\mathrm{nf}_0}$.

D. Hardware Requirements

The RHC of our *RC* MASH DDSM designed with the zero-order dither technique compared with the conventional DDSM is

$$RHC_0 \approx \frac{N + \mathrm{ceil}(0.67N) + \mathrm{ceil}\,(0.33N)}{3N} \times 100\%. \quad (61)$$

RHC_0 approaches 67% for large N's. However, due to the fact that dithering consumes some additional hardware, the percentage hardware saving of the DDSM plus dither generator is less.

In the same manner, the RHC of our *RC* MASH DDSM designed with first-order dither and a 3-dB guard band compared with the conventional DDSM is

$$RHC_1 = \frac{N + N + \mathrm{ceil}(0.5N + 0.5)}{3N} \approx \frac{2.5N + 0.5}{3N} \times 100\%. \quad (62)$$

Asymptotically, RHC_1 approaches 83% for large N's. For the 14-bit case, (62) predicts that our *RC* implementation will require 15% less hardware.

VI. Design Example (With Dither)

A design example for a zeroth-order dithered 20-bit MASH DDSM is discussed in this section. Applying design equations (50) and (51), the appropriate word lengths of the second and third stages of the *RC* DDSM are 14 and 7, respectively. A 20–14–7 *RC* DDSM is simulated to show typical contributions N_{12}, N_{23}, and N_3 (see Figs. 27–29). The dither cycle length is 2^{24}.

A. Simulations

The simulated PSD for a conventional zeroth-order dithered 20-bit MASH 111 DDSM is shown in Fig. 30.

The PSD of the *RC* 20–14–7-bit equivalent is shown in Fig. 31. Note that the N_{12} and N_{23} components lie below the

Authorized licensed use limited to: UNIVERSITY COLLEGE CORK. Downloaded on March 26,2010 at 12:10:11 EDT from IEEE Xplore. Restrictions apply.

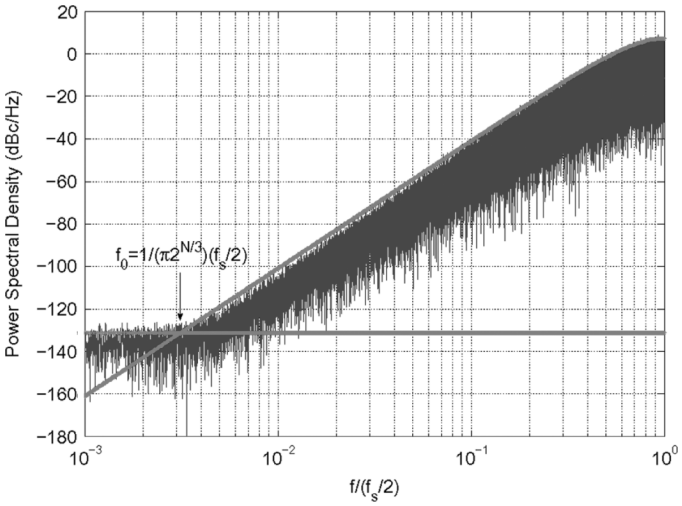

Fig. 31. Simulated PSD at the output of a zeroth-order dithered *RC* 20-14-7-bit MASH 111 DDSM; the input is 104 857 (Compare with Fig. 30).

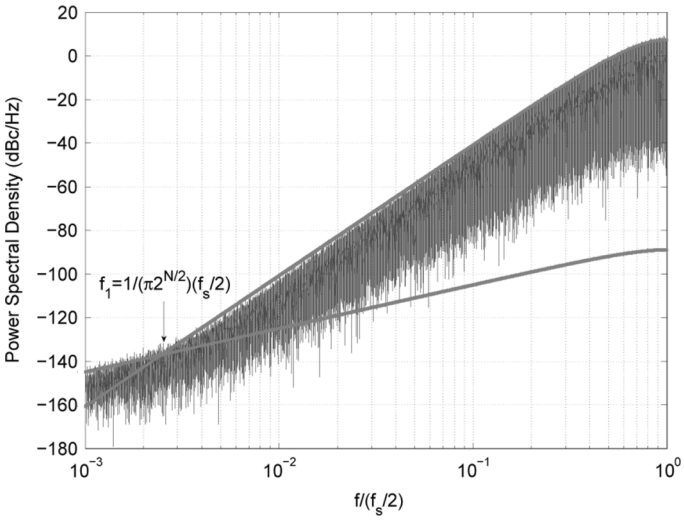

Fig. 32. Simulated PSD at the output of a conventional first-order dithered 14-bit MASH 111 DDSM; the input is 1639. The dc term has been removed. The solid curves are $\mathcal{L}_3$ and $\mathcal{L}_{nf_1}$.

spectral envelope of N_3 and are therefore masked by it, as expected. Consequently, N_{12} and N_{23} do not affect the overall performance of the *RC* DDSM.

The simulated PSD for a conventional 14-bit MASH 111 DDSM with first-order additive input dither is shown in Fig. 32.

Applying the design (60), the word length of the third stage of the *RC* DDSM is eight. The simulated PSD for the *RC* 14–14–8 MASH 111 DDSM is shown in Fig. 33. As expected, the *RC* DDSM achieves an almost identical PSD compared to the conventional 14-bit DDSM.

B. RHC

The hardware requirements for: 1) a conventional 20-bit MASH 111 DDSM with zeroth-order dither; 2) an *RC* 20–14–7 DDSM with zeroth-order dither; 3) a conventional 14-bit MASH 111 DDSM with first-order dither; and 4) an *RC* 14–14–8 MASH DDSM with first-order dither are summarized in Table II.

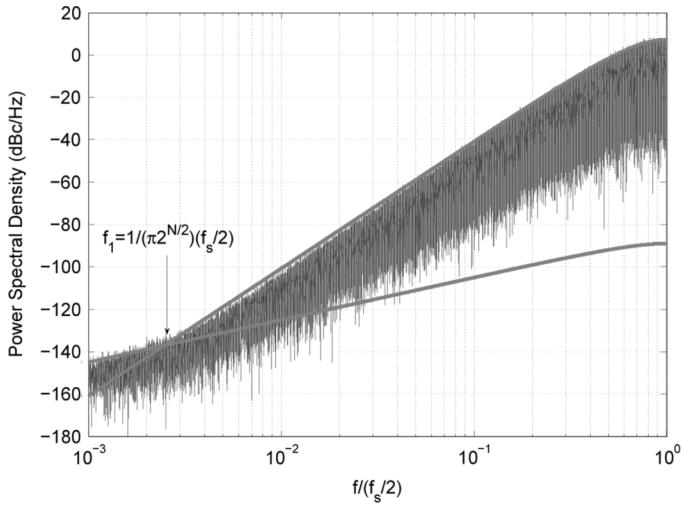

Fig. 33. Simulated PSD for a first-order dithered *RC* 14–14–8-bit MASH 111 DDSM; the input is 1639 (Compare with Fig. 32).

TABLE II
HC OF THE CONVENTIONAL 20-BIT MASH 111 DDSM AND THE 20–14–7-BIT *RC* DDSM WITH ZEROTH-ORDER DITHER AND THE 14-BIT MASH 111 DDSM AND THE 14–14–8-BIT *RC* DDSM WITH FIRST-ORDER DITHER

MASH DDSM with dither	Hardware Consumption		
	FFs	LUTs	TEGs
(a) 20 bit with zeroth-order dither	139	91	1931
(b) 20-14-7 bit with zeroth-order dither	101	66	1375
((b)/(a))%	73%	73%	71%
(c) 14 bit with first-order dither	109	67	1435
(d) 14-14-8 bit with first-order dither	97	61	1307
((d)/(c))%	89%	91%	89%

The 20–14–7 *RC* MASH DDSM with zeroth-order dither achieves an almost identical PSD to the 20-bit conventional DDSM with dithering, but with 29% less hardware. If we subtract the HC for the dither block for both MASH DDSMs, which is 266 TEG, our *RC* MASH DDSM has an RHC of 67%, as predicted by (61). For the first-order dither case, our 14–14–7 DDSM consumes 89% hardware compared with the conventional 14-bit *RC* DDSM. In the same manner, if we exclude the consumption of the dither block, the RHC for our *RC* DDSM is 86% of the conventional DDSM, as predicted by (62).

VII. CONCLUSION

In this paper, we have presented a design methodology for MASH DDSMs based on error masking. We have shown that, starting with a conventional DDSM, it is possible to find an optimized word length for each stage of the DDSM, which allows a reduction in the HC by up to 20%, without degrading the spectral performance. Our simulation and experimental results confirm our analytical predictions. In the second part of this paper, we will extend our methodology to SQ DDSMs [14].

REFERENCES

[1] S. R. Norsworthy, R. Schreier, and G. C. Tames, *Delta–Sigma Data Converters*. New York: IEEE Press, 1997.
[2] V. Friedman, "The structure of the limit cycles in sigma delta modulation," *IEEE Trans. Commun.*, vol. 35, pp. 784–796, Jul. 1989.

Authorized licensed use limited to: UNIVERSITY COLLEGE CORK. Downloaded on March 26,2010 at 12:10:11 EDT from IEEE Xplore. Restrictions apply.

[3] M. Kozak and I. Kale, "Rigorous analysis of delta–sigma modulator for fractional-N PLL frequency synthesis," *IEEE Trans. Circuits and Systems I: Regular Papers*, vol. 51, no. 6, pp. 1148–1162, Jun. 2004.
[4] M. J. Borkowski, T. A. D. Riley, J. Hakkinen, and J. Kostamovaara, "A practical $\Delta\Sigma$ modulator design method based on periodical behavior analysis," *IEEE Trans. Circuits and Systems II: Express Briefs*, vol. 52, no. 10, pp. 626–630, Oct. 2005.
[5] K. Hosseini and M. P. Kennedy, "Mathematical analysis of digital MASH delta–sigma modulator for fractional-N frequency synthesizers," in *Proc. of PRIME 2006*, Otranto, Italy, Jun. 2006, pp. 309–312.
[6] S. Pamarti and I. Galton, "LSB dithering in MASH delta–sigma D/A converters," *IEEE Trans. Circuits and Systems I*, vol. 54, no. 4, pp. 779–790, Apr. 2007.
[7] Z. Ye and M. P. Kennedy, "Reduced complexity MASH delta–sigma modulator," *IEEE Trans. Circuits Syst. II, Exp. Briefs*, vol. 54, no. 8, pp. 725–729, Aug. 2007.
[8] L. A. Williams and F. Cavaliere, "Reduced Area Digital Sigma–Delta Modulator," US Patent US 7 176 821 B1, Feb. 2007.
[9] M. Kozak and I. Kale*, Oversampled Delta–Sigma Modulators—Analysis, Applications and Novel Topologies*. : Kluwer Academic Publishers, 2003.
[10] T. A. Riley, M. Copeland, and T. Kwasniewski, "Delta–sigma modulation in fractional-N frequency synthesis," *IEEE J. Solid-State Circuits*, vol. 28, pp. 553–559, May 1993.
[11] M. P. Kennedy and Z. Ye, "A Delta Sigma Modulator," Irish Patent, application number 2006/0763, Oct. 17, 2006.
[12] S. Haykin and B. D. Van Veen*, Signals and Systems*, 2nd ed. New York: John Wiley and Sons, 2003.
[13] *ISE Quick Start Tutorial*, , 2005 [Online]. Available: http://toolbox.xilinx.com/docsan/xilinx7/books/docs/qst/qst.pdf, [online]. Available
[14] Z. Ye and M. P. Kennedy, "Hardware reduction in digital delta-sigma modulators via error masking—Part II: SQ-DDSM," *IEEE Trans. Circuits Syst. II, Exp. Briefs*, vol. 56, no. 2, pp. 112–116, Feb. 2009.

Zhipeng Ye (S'05) was born in 1981. He received the B.E. degree in control science and engineering from Harbin Institute of Technology, Harbin, China, in 2004 and the M.Eng.Sc. and Ph.D. degrees from the University College Cork and Tyndall National Institute, Cork, Ireland, in 2005 and 2008, respectively.

He is currently with Australian Semiconductor Technology Corporation (ASTC), Pty Ltd., Adelaide, South Australia. He is the holder of one patent on digital delta–sigma modulators. His research interests are in the areas of modeling, simulation, and design of fractional-N.

Dr. Ye was the recipient of the Bronze Leaf Certificate at the Third Conference on Ph.D. Research in Microelectronics and Electronics 2007, the Microsoft Best Paper Award at the 2007 China–Ireland International Conference on Information and Communications Technologies, and the Gold Leaf Certificate at the Fourth Conference on Ph.D. Research in Microelectronics and Electronics 2008.

Michael Peter Kennedy (S'84–M'91–SM'95–F'98) received the B.E. degree in electronics from the National University of Ireland, Dublin, Ireland, in 1984 and the M.S. and Ph.D. degrees from the University of California (UC Berkeley), Berkeley, in 1987 and 1991, respectively.

He was a Design Engineer with Philips Electronics, a Postdoctoral Research Engineer with the Electronics Research Laboratory, UC Berkeley, and a Professeur Invité at the Federal Institute of Technology Lausanne, Lausanne, Switzerland. From 1992 to 2000, he was with the faculty of the Department of Electronic and Electrical Engineering, University College Dublin, Dublin, Ireland, where he taught electronic circuits and computer-aided circuit analysis and directed the undergraduate Electronics Laboratory. Since 2000, he has been with the University College Cork (UCC), Cork, Ireland, as Professor and Head of the Department of Microelectronic Engineering, Faculty of Engineering. He was appointed Dean of Faculty of Engineering in 2003 and Vice-President for Research in 2005. He is also with Tyndall National Institute, Cork. He has published over 260 papers in the area of nonlinear circuits, is the holder of six patents, and has taught courses on nonlinear dynamics and chaos in England, Switzerland, Italy, and Hungary. His research interests are in the simulation, analysis, and design of nonlinear dynamical systems for applications in communications and signal processing.

Dr. Kennedy was made an IEEE Fellow for his contributions to the study of neural networks and nonlinear dynamics. He was the Associate Editor of the IEEE TRANSACTIONS ON CIRCUITS AND SYSTEMS from 1993 to 1995 and from 1999 to 2004. He was Vice President for Region 8 of the IEEE Circuits and Systems Society from 2005 to 2007. He was the recipient of the 1991 Best Paper Award from the International Journal of Circuit Theory and Applications and the Best Paper Award at the European Conference on Circuit Theory and Design 1999. He was the recipient of the IEEE Third Millennium Medal, the IEEE Circuits and Systems Society Golden Jubilee Medal in 2000, and the inaugural Parsons Medal for Engineering Sciences by the Royal Irish Academy in 2001. He was elected to membership of the Royal Irish Academy in 2004.

Authorized licensed use limited to: UNIVERSITY COLLEGE CORK. Downloaded on March 26,2010 at 12:10:11 EDT from IEEE Xplore. Restrictions apply.